DOI: 10.13208/j.electrochem.161249 **Artical ID**:1006-3471(2017)02-0199-08
Cite this: *J. Electrochem.* **2017**, *23*(2): 199-206 **Http**://electrochem.xmu.edu.cn

Comparison of Oxygen Reduction Reaction Activity of Pt-Alloy Nanocubes

Yongan Tang[1,3], Lin Dai[1], Shouzhong Zou[1,2*]
(1. *Department of Chemistry and Biochemistry, Miami University, Oxford, OH* 45056,*USA*;
2. *Department of Chemistry, American University, Washington DC* 20016, *USA*;
3. *Department of Chemistry, Oakland University, Rochester, MI* 48039, *USA*)

Abstract: Alloying Pt with the first row non-noble transition metals has been demonstrated to increase the catalytic activity toward oxygen reduction reaction (ORR), which is the cathode reaction of the proton exchange membrane fuel cells (PEMFCs) and metal-air batteries. However, how much the ORR activity improvement comes from the alloying elements remains controversial. In this paper, the nanocubes of PtMn, PtFe, PtCo, and PtNi with the similar size and composition were prepared and their ORR activities were explored, in order to investigate the effects of alloying elements on the catalytic activity. The use of cubic shape particles minimizes the contribution to the activity from particle surface structural difference. The results showed that the ORR activity vs. Pt d-band center plot had a volcano shape and PtCo nanocube is the most active. These observations are in harmony with density functional theory calculations on well-defined surfaces in the framework of the d-band theory.

Key words: Pt-alloy nanocubes; oxygen reduction reaction; proton exchange membrane fuel cells; d-band theory
CLC Number: O646 **Document Code**: A

Fuel cells are promising power sources for vehicles and portable electronic devices due to their environmentally friendly nature and high energy conversion efficiency. Among many technical challenges, the sluggish kinetics of oxygen reduction reaction (ORR), the high cost of Pt, and the vulnerability of Pt electrocatalyst toward reaction poisons significantly hinder the widespread applications of proton exchange membrane fuel cells (PEMFCs)[1-2]. Therefore, developing inexpensive, highly active and poison resistant catalysts for ORR is an active research area. In this regard, Pt alloy nanoparticles have attracted increasing interests because of their higher ORR activi ty compared to pure Pt[2]. The presence of a second transition metal alters the electronic structure of Pt, and therefore, changes its adsorption property and catalytic activity. In fact, significantly improved ORR activity has been reported on Pt alloyed with less expensive 3d-transition metals (PtM, M = Mn[3], Fe[4-5], Co[6-7], Ni[3,8], etc.). However, there are significant inconsistencies in the magnitude of ORR activity improvement of Pt-based bimetallic alloys in the literature. For example, Toda et al.[9] reported an up to 10-time enhancement of ORR activity on Pt-Ni, Pt-Co and Pt-Fe catalysts over the pure Pt, but less than 3-fold improvement was observed on Pt-Co and Pt-Ni by Paulus et al[10].

Different periodic trends of ORR activity have also been reported on Pt alloys[11]. Sometime ago, Mukerjee et al. reported a volcano shape plot of specific activity of Pt-based alloys (PtCr, PtMn, PtFe, PtCo, PtNi) versus alloying elements and PtFe lied at the top of the curve[5]. However, Pt_3Ni and Pt_3Co have the highest catalytic activity, respectively, based on theoretical calculations[12] and experimental results on macroscopic Pt_3Ti, Pt_3Fe, Pt_3Co, Pt_3Ni, and Pt surfaces prepared under ultra high vacuum[4]. Others reported similar specific ORR activities on PtFe, PtCo and Pt-Ni nanoparticles after 1200 potential cycles between 0.6 and 1.0 V vs. RHE in Ar-saturated 0.10 mol·L^{-1}

Received: 2017-01-13, Revised: 2017-02-17 *Corresponding author, Tel: (001-202)8851763, E-mail: szou@american.edu

$HClO_4$[13]. It has been demonstrated that ORR activity is not only affected by the second metal in Pt-based alloy catalyst[4], but also strongly depends on the particle surface structure[14] and composition[15-17]. The above discrepancies may arise from the different shapes, sizes, and compositions of the Pt-based alloy nanoparticles. In order to minimize these confounding factors and reveal the effects of the alloying metal on the ORR activity, it is critical to control the structure and composition of the particles.

The synthesis of different Pt-based bimetallic alloy nanoparticles with well controlled shapes has been advanced rapidly recently[18-19]. Taking advantage of this progress, we synthesized the monodispersed Pt-based bimetallic nanocubes (PtMn, PtFe, PtCo, and PtNi), which are enclosed by {100} facets, at elevated temperatures in organic solutions, and compared their ORR activity with Pt nanocubes of similar size. Among these nanocubes, PtCo exhibited the highest ORR activity, which can be explained by its optimal Pt d-band center energy. Because of the well-controlled structure of the nanocubes used in this study, the observed catalytic activity difference can be safely attributed to the alloying elements.

1 Experimental

1.1 Synthesis and Characterization of Pt-Alloy Nanocubes

The Pt and Pt-based alloy nanocubes (NCbs) including PtMn, PtFe, PtCo and PtNi were prepared by utilizing previously reported methods[18,20]. Brief synthesis procedures are described in the following. For synthesizing PtFe and PtCo NPs, 0.020 g of platinum (II) acetylacetonate (98%, Acros Organics), 0.010 g of iron(II) chloride tetrahydrate (99.99%, Aldrich) or 0.0125 g of cobalt acetate tetrahydrate (99.999%, Aldrich), 8.0 mL of oleylamine (80% ~ 90%, Acros Organics), and 2.0 mL of oleic acid (90%, Aldrich) were loaded into a three-neck flask. The mixture was purged with nitrogen gas for 10 min before it was heated to 130 ℃ in an oil bath with continuous stirring under the nitrogen stream. Next, 0.050 g of tungsten hexacarbonyl (97%, Aldrich) was added to the solution, and the temperature was raised to 240 ℃ and reacted for 40 min at this temperature. We found that the stir rate is an important parameter that influences the shape of the particles. In this work, 85 $r \cdot min^{-1}$ stir rate was typically used. The synthesis procedure of PtNi is similar to those of PtFe and PtCo. The only difference is that the Ni precursor (0.4 mL $NiCl_2$ solution which was prepared by dissolving 0.238 g of nickel(II) chloride hexahydride (99.95%, Alfa Aesar) into 5.0 mL of oleylamine and 5.0 mL of oleic acid) was added to the reaction mixture after the tungsten hexacarbonyl was added. It is worth pointing out that the injection rate of Ni precursor also plays an important role in the shape control. The optimal injection rate was one drop per 15 seconds controlled by a syringe (1 mL, 27 gauge). During the injection of Ni precursor, the temperature was raised from 130 ℃ to 200 ℃. After the Ni precursor injection, the temperature was further increased to 240 ℃ and reacted for 15 min. The PtMn NCbs were synthesized as follows. 0.040 g of platinum(II) acetylacetonate was dissolved in a mixture of 5 mL of benzyl ether (99%, Acros Organics), 3.68 mL of oleylamine, and 0.63 mL of oleic acid. The solution was purged with nitrogen for 10 min and then the reaction flask was placed into an oil bath preheated to 200 ℃. 3.5 mL of manganese(0) decacarbonyl stock solution prepared by dissolving 0.078 g manganese(0) carbonyl (98%, from Aldrich) in 20.0 mL of benzyl ether was injected to the reaction mixture once the temperature reached 160 ℃. The reaction was allowed to run at 200 ℃ for 30 min. Before microscopic measurements, the as-synthesized nanoparticles were washed with hexane and ethanol by repetitive centrifugation and dispersion to remove majority of the surfactants. The cleaned particles were redispersed in the same volume of hexane by sonication. Transmission elec tron microscopic (TEM) images of the washed particles without subject to potential cycling treatment were obtained using a JEOL JEM-1200 microscope at an accelerating voltage of 120 kV. The composition of the NCbs was determined by using an inductively coupled plasma optical emission spectrometer (ICP-OES, Optima 7300 DV, Perkin Elmer). The sam-

ples for determination of the Pt/M ratio before electrochemical potential cycling were prepared by placing 15 μL of the nanoparticle suspension to a fresh aqua regia to dissolve the particles overnight. For the determination of the Pt/M ratio after the potential cycling, 15 μL of the nanoparticle suspension was drop-coated on a glassy carbon (GC) disk electrode and the nanoparticles were digested after the electrochemical measurements in a freshly prepared aqua regia overnight. The obtained solution was diluted 20 times by water before ICP-OES measurements.

1.2 Preparation of Carbon Supported Electrocatalysts

To make carbon supported Pt-alloy or Pt nanocube electrocatalysts, the particle suspension in hexane was dried in air and weighed. Carbon black (Cabot Corporation) with the same weight as that of dry NCbs was dispersed in a mixture of ethanol and hexane, and sonicated for one hour. The carbon supported Pt-alloy (or Pt) NCbs were prepared by mixing the carbon black suspension and the particles dropwise. The resultant solution was stirred vigorously overnight to form a catalyst with a nominal 50%(by mass) metal loading. To further remove the residual organic surfactants on the particles before electrochemical studies, the PtM/C (or Pt/C) electrocatalyst were subject to a thermal annealing treatment at 185 ℃ in air for 45 min followed by a second thermal annealing treatment at 300 ℃ in N_2 atmosphere for an other 45 min. The 1 mg Pt-alloy/C (or Pt/C) per mL electrocatalyst suspension was prepared by dispersing the thermally treated Pt-alloy/C (or Pt/C) in the mixture of water, isopropanol, and Nafion solution (5wt% in water/alcohol mixture) with a volume ratio of water, isopropanol, and Nafion solution being 4:1:0.025.

1.3 Electrochemical Measurements

To study the electrochemical properties of these nanocubes, cyclic voltammograms (CVs) and polarization curves (RDE) were recorded in 0.10 $mol \cdot L^{-1}$ $HClO_4$ solutions with a conventional two-compartment three-electrode cell using a CHI 700B electrochemical analyzer. A Pt wire served as the counter electrode, and a KCl-saturated Ag/AgCl electrode was used as the reference electrode. However, all of the electrode potentials were reported with respect to a reversible hydrogen electrode. The working electrode was prepared by drop-coating 15 μL of PtM/C (or Pt/C) suspension on a GC electrode (geometric area: 0.196 cm^2). The nominal Pt loading was 6.8 μg for all of the PtM/C catalysts, and 6.0 μg for Pt/C. The cell resistance was compensated with the iR compensation function in the analyzer. The Pt surface areas of the catalysts were determined electrochemically by CO stripping charge assuming the charge for oxidation of a monolayer of adsorbed CO is 0.420 $mC \cdot cm^{-2}$[21]. The CO stripping experiments were carried out as follows: after the adsorption of CO under potentiostatic control at 0.16 V for a period of 5 min the cell was flushed with N_2 for 20 min to remove un-adsorbed CO and finally the potential was scanned at 100 $mV \cdot s^{-1}$. All of the solutions were prepared using water purified by a Milli-Q system with a resistivity of 18.2 $M\Omega \cdot cm$. All of the measurements were made at room temperature (22 ± 1 ℃).

2 Results and Discussion

The shape of Pt-based nanocubes was first examined using TEM as shown in Figure 1 (A-E). The images clearly reveal the feature of cubic shape of these particles. The average side-lengths are all around 9 ± 1 nm. The percent of particles that are nanocube is 80% ~ 90%. The similar size of these Pt and Pt-based bimetallic catalysts ensures the ORR activity comparison without the complication of the size effect[22-23].

The surface of the as-prepared NCbs is covered partially by the surfactants used in the synthesis to control the size and shape, as manifested by the absence of diminishing hydrogen adsorption/desorption peaks characteristics of well-defined surfaces[24-25]. These surfactants obscure the catalytic activity studies. Effective removal of these surfactants is a prerequisite of using these NCbs as model catalysts[24-25]. By annealing the NCbs in vacuum or an inert atmosphere (N_2, Ar, etc.), the surfactants can be largely removed. Prior to electrochemical characterizations, the as-pre-

pared NCbs were subject to a thermal annealing treatment at 185 ℃ in air for 45 min followed by thermal annealing at 300 ℃ in N_2 for another 45 min. The effects of thermal annealing treatments were manifested by the appearance or increase of hydrogen adsorption/desorption peaks in CVs obtained in 0.10 mol·L^{-1} $HClO_4$. No obvious size or morphology change was observed for the NCbs after the thermal treatments, as shown by the TEM image of the annealed Pt NCbs/C in Figure 1(F), and PtCo NCbs/C in Figure 2. The upper limit of the annealing temperature at 300 ℃ was set by the deterioration of the cubic shape above this temperature.

To evaluate their electrocatalytic activity, the NCbs/C were drop-coated on a GC electrode after they were thermally treated and dispersed in the mixture of water, isopropanol, and Nafion solution as described in the experimental section. Before CVs and ORR polarization curves were recorded, these NCbs were subject to potential cycling between 0.05 and 1.0 V for 100 cycles in 0.10 mol·L^{-1} $HClO_4$ to further clean the particle surface. Figure 3 presents the CVs of PtM and Pt NCbs/C on a GC electrode in deaerated 0.10 mol·L^{-1} $HClO_4$. Two pairs of hydrogen adsorption/desorption peaks at ~ 0.27 V and ~ 0.38 V

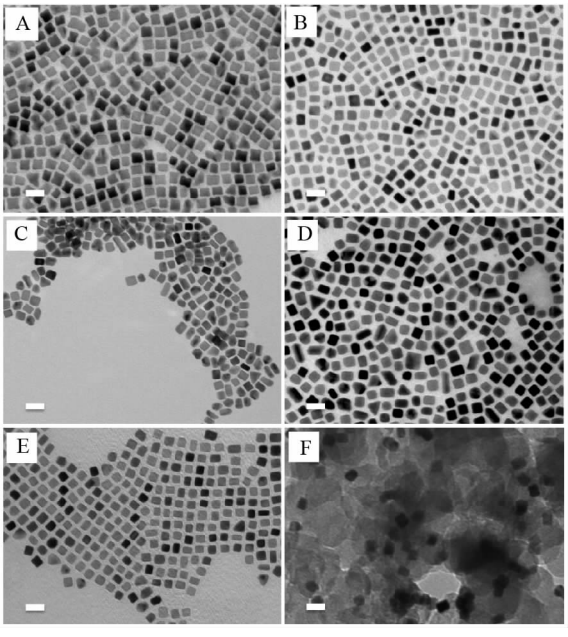

Fig. 1 TEM images of PtM and Pt NCbs (Scale bar: 20 nm.)
A.PtMn; B. PtFe; C.PtCo; D. PtNi; E-F. Pt andPt/C

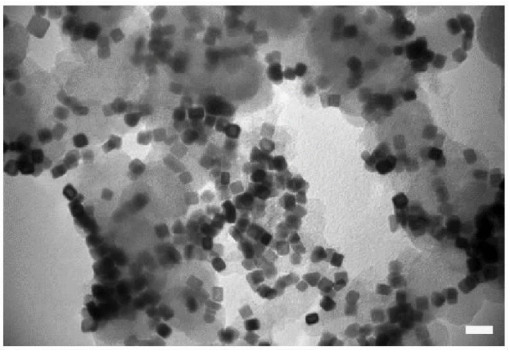

Fig. 2 TEM image of PtCo NCbs/C after 300 ℃ annealing (Scale bar: 20 nm)

were clearly evident, suggesting the dominance of the {100} facet on these nanocubes[26]. These current features also suggest the cleanness of the NCb surfaces after the pretreatment processes[25].

The ICP-OES measurements were performed to monitor the particle composition before and after the potential cycling (PC) pretreatments, and the results are summarized in Table 1. All of the as-synthesized PtM alloys have a similar Pt to M ratio of 3 to 1. However, the ratio increased to about 4 to 1 after the electrochemical cycling pretreatment. The Pt/M ratio increase after the potential cycling indicates that part of the M in the alloy NCbs was leached out and a Pt-rich NCbs surface was formed. The presence of a Pt-rich surface is supported by the observation of characteristic hydrogen adsorption/desorption peaks on Pt{100}. Further support of this notion comes from

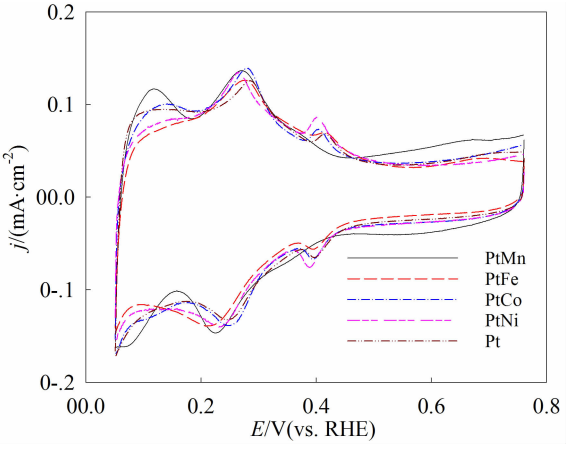

Fig. 3 Cyclic voltammograms of PtM and Pt NCbs/C in 0.10 mol·L^{-1} $HClO_4$ solution (Scan rate: 100 mV·s^{-1})

the surface sensitive carbon monoxide oxidation. The CO oxidation peaks in the stripping voltammograms obtained on Pt alloys nearly overlap with that from pure Pt NCbs (Figure 4). Were there abundant transition elements on the catalyst surfaces, the CO stripping peak would be more negative than that on the pure Pt[27]. Based on the amount of alloying element lost and the size of the particles, the dealloying is estimated to occur only on the top two atomic layers of the particles. The hydrogen adsorption/desorption and CO oxidation peaks characteristics of {100} facets are clearly observed in the CVs (Figures 3 and 4), suggesting that the surface structures were not seriously disrupted by the dissolution of the less noble alloying element[25]. In fact, the appearance of the CO stripping peak near ~ 0.77 V and the absence of a shoulder peak at around 0.72 V are indicative of the absence of significant amount of defect sites on these nanocubes[25].

Rotating disk electrode (RDE) voltammetry was used to examine the effects of different transition metals on ORR kinetics of PtM electrocatalysts. A typical set of polarization curves obtained on Pt and the four PtM NCbs in an O_2-saturated 0.10 mol·L^{-1} $HClO_4$ solution at 295 K are presented in Figure 5. The results show that the ORR activity is strongly dependent on the different transition metals. The kinetic current was evaluated by using the Koutecky-Levich equation:

$$\frac{1}{I}=\frac{1}{I_K}=\frac{1}{I_l} \tag{1}$$

where I is the current at a given potential, I_k is the kinetic current at this potential, and I_l is the limiting current at the plateau. The area specific ORR activity was obtained by normalizing the kinetic current to the catalyst surface area estimated from the CO oxidation charge. Consistent with previous studies, all of the PtM NCbs showed higher ORR activity than Pt NCbs[3-5, 12-13]. The specific ORR activity measured at 0.85 V is plotted against the d-band center energy and a volcano shape plot is obtained (Figure 6). The specific activity was reported at 0.85 V instead of the more commonly used 0.90 V to avoid large uncertainties in ORR activity at the latter potential due to the significantly lower current. It is known that Pt (100) single crystal surfaces are significantly less active than Pt(111) surfaces for ORR in acidic media[28]. The PtCo NCbs shows the highest ORR activity, which is more than two times of that from Pt NCbs. Similarly, the PtCo also has the highest mass activity,

Tab. 1 Compositions of PtM NCbs before and after potential cycling (PC) pretreatments

	PtMn	PtFe	PtCo	PtNi
Pt:M mole ratio before PC	2.8	3.2	2.8	2.9
Pt:M mole ratio after PC	4.0	4.2	3.9	4.3

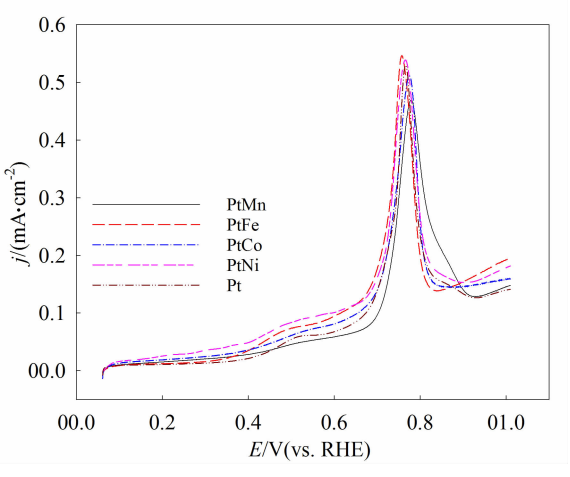

Fig. 4 CO stripping voltammograms obtained on PtM and Pt NCbs/C in 0.10 mol·L^{-1} $HClO_4$. Scan rate: 100 mV·s^{-1}

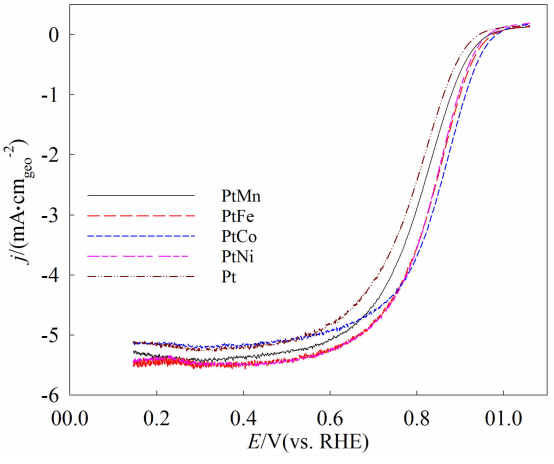

Fig. 5 Polarization curves for ORR on PtM and Pt NCbs/C supported on a rotating GC disk electrode in O_2 saturated 0.10 mol·L^{-1} $HClO_4$ solution at 295 K. Scan rate: 20 mV·s^{-1}, rotation rate: 1600 r·min^{-1}

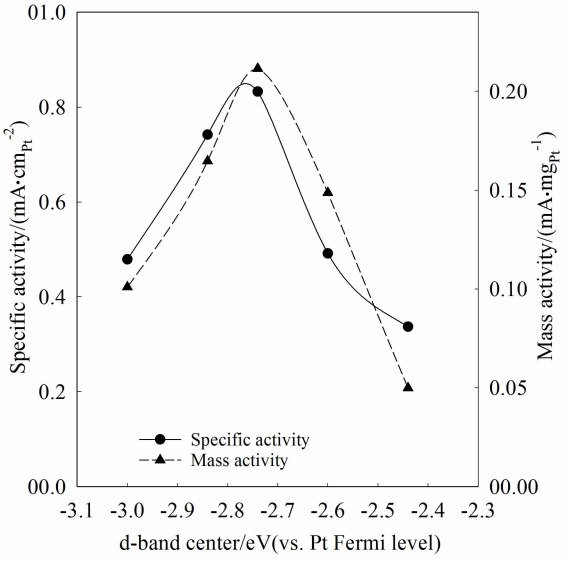

Fig. 6 Relationship between ORR activities measured at 0.85 V and the calculated d-band center values for Pt and PtM catalysts. The d-band center values were taken from ref.[29].

which was measuredas the kinetic current at 0.85 V normalized to the Pt mass in the NCbs.

The trend of ORR activity on these cubes agrees well with that observed by Stamenkovic et al. on macroscopic Pt_3M (M = Ti, Fe, Co and Ni) surfaces prepared under ultrahigh vacuum[4], but differs from those reported by others[3, 5, 13]. The difference may be attributed to the well-controlled surface structure used in the present work and in Stamenkovic et al[4]. To the best of our knowledge, ORR activity comparison on facet-controlled nanocrystals of PtM has not been reported before. The observed trend can be understood in the framework of the d-band theory[29]. At the center of this theory is that the adsorption energy of a species is proportional to the metal d-band center (i.e. average d-band energy) and the d-band center can be tuned by alloying with a second metal through the electronic and strain effects[29]. It has been shown both experimentally and theoretically that for Pt_3M alloys (M = the first row transition metals) with a Pt top layer (the so called "Pt-skin") the d-band center of the Pt top layer is lower than the pure Pt, and the adsorption energy consequently decreases[4,29]. Through density function theory (DFT) calculations it was shown that the oxygen adsorption energy on various Pt skins is linearly proportional to the d-band center position[12]. Therefore the adsorption energy of oxygen on PtM is lower than that on Pt. According to the Sabatier principle[30], for metal surfaces that strongly bind oxygen on their surfaces, the ORR rate is limited by the removal of adsorbed O(ads) or H_2O_2(ads) species. These species will oxidize the metal surface and block the reactivity of oxygen reduction[31]. For metals that bind oxygen too weakly, the ORR rate is restricted by the slow dissociation of O_2(ads). Under this context, the d-band center for pure Pt is too high, and therefore, Pt binds oxygen too strongly, while the d-band center for PtMn is too low and the ORR is limited by the slow O_2 dissociation. The highest ORR activity observed on PtCo nanocubes is a manifestation of the most suitable d-band energy among different alloy metals.

3 Conclusions

In summary, four Pt-based binary alloy NCbs as well as pure Pt NCbs have been synthesized and used for comparing alloy effects of early transition metals on the ORR activity in 0.10 mol·L^{-1} $HClO_4$. These nanocubes enable the study of effects of the nature of the alloying transition metals on the ORR activity without the complications of other structural variations such as size and shape. Our results clearly demonstrate that ORR activity strongly depends on the alloyed elements. The activity is governed by the strength of the oxygen-metal interaction, which in turn depends on the metal d-band energy center. The PtCo has the most optimal d-band energy which results in the highest ORR activity among four transition metals we tested here. The results provide experimental data that may stimulate further theoretical work beyond {111} facets, and more importantly, demonstrate that searching for surfaces with appropriate oxygen binding energy is an effective way for developing highly active ORR catalysts.

Acknowledgements

This work was supported by the US National Science Foundation (CHE 1156425, CHE 1559670).

References:

[1] Vielstich W, Lamm A, Gasteiger H A. Handbook of fuel cells: Fundamentals, technology, applications[M]. Wiley: New York, 2003.

[2] Gasteiger H A, Kocha S S, Sompalli B, et al. Activity benchmarks and requirements for Pt, Pt-alloy, and non-Pt oxygen reduction catalysts for PEMFCs[J]. Applied Catalysis B-Environmental, 2005, 56(1/2): 9-35.

[3] Mukerjee S, Srinivasan S. Enhanced electrocatalysis of oxygen reduction on platinum alloys in proton-exchange membrane fuel-cells[J]. Journal of Electroanalytical Chemistry, 1993, 357(1/2): 201-224.

[4] Stamenkovic V R, Mun B S, Arenz M, et al. Trends in electrocatalysis on extended and nanoscale Pt-bimetallic alloy surfaces[J]. Nature Materials, 2007, 6(3): 241-247.

[5] Mukerjee S, Srinivasan S, Soriaga M P, et al. Role of structural and electronic-properties of Pt and Pt alloys on electrocatalysis of oxygen reduction - an *in-situ* XANES and EXAFS investigation[J]. Journal of the Electrochemical Society, 1995, 142(5): 1409-1422.

[6] Watanabe M, Tsurumi K, Mizukami T, et al. Activity and stability of ordered and disordered Co-Pt alloys for phosphoric-acid fuel-cells[J]. Journal of the Electrochemical Society, 1994, 141(10): 2659-2668.

[7] Koh S, Leisch J, Toney M F, et al. Structure-activity-stability relationships of Pt-Co alloy electrocatalysts in gas-diffusion electrode layers[J]. Journal of Physical Chemistry C, 2007, 111(9): 3744-3752.

[8] Stamenkovic V, Schmidt T J, Ross P N, et al. Surface segregation effects in electrocatalysis: kinetics of oxygen reduction reaction on polycrystalline Pt_3Ni alloy surfaces[J]. Journal of Electroanalytical Chemistry, 2003, 554:191-199.

[9] Toda T, Igarashi H, Uchida H, et al. Enhancement of the electroreduction of oxygen on Pt alloys with Fe, Ni, and Co[J]. Journal of the Electrochemical Society, 1999, 146: 3750-3756.

[10] Paulus U A, Wokaun A, Scherer G G, et al. Oxygen reduction on carbon-supported Pt-Ni and Pt-Co alloy catalysts[J]. Journal of Physical Chemistry B, 2002, 106(16): 4181-4191.

[11] Bing Y H, Liu H S, Zhang L, et al. Nanostructured Pt-alloy electrocatalysts for PEM fuel cell oxygen reduction reaction[J]. Chemical Society Reviews, 2010, 39(6): 2184-2202.

[12] Stamenkovic V, Mun B S, Mayrhofer K J J, et al. Changing the activity of electrocatalysts for oxygen reduction by tuning the surface electronic structure[J]. Angewandte Chemie-International Edition, 2006, 45(18): 2897-2901.

[13] Han B, Carlton C E, Suntivich J, et al. Oxygen reduction activity and stability trends of bimetallic $Pt_{0.5}M_{0.5}$ nanoparticle in acid[J]. The Journal of Physical Chemistry C, 2015, 119(8): 3971-3978.

[14] Zhang J, Yang H Z, Fang J Y, et al. Synthesis and oxygen reduction activity of shape-controlled Pt_3Ni nanopolyhedra[J]. Nano Letters, 2010, 10(2): 638-644.

[15] Zhang C, Hwang S Y, Trout A, et al. Solid-state chemistry-enabled scalable production of octahedral Pt-Ni alloy electrocatalyst for oxygen reduction reaction[J]. Journal of the American Chemical Society, 2014, 136(22): 7805-7808.

[16] Choi S I, Xie S, Shao M, et al.Controlling the size and composition of nanosized Pt-Ni octahedra to optimize their catalytic activities toward the oxygen reduction reaction[J]. ChemSusChem, 2014, 7(5): 1476-1483.

[17] Chou S W, Lai Y R, Yang Y Y, et al. Uniform size and composition tuning of PtNi octahedra for systematic studies of oxygen reduction reactions[J]. Journal of Catalysis, 2014, 309: 343-350.

[18] Zhang J, Fang J Y. A general strategy for preparation of Pt 3d-transition metal (Co, Fe, Ni) nanocubes[J]. Jour nal of the American Chemical Society, 2009, 131(51): 18543-18547.

[19] Gilroy K D, Ruditskiy A, Peng H C, et al. Bimetallic nanocrystals: Syntheses, properties, and applications[J]. Chemical Reviews, 2016, 116(18): 10414-10472.

[20] Kang Y J, Murray C B. Synthesis and electrocatalytic properties of cubic Mn-Pt nanocrystals (nanocubes)[J]. Journal of the American Chemical Society, 2010, 132(22): 7568-7569.

[21] Maillard F, Eikerling M, Cherstiouk OV, et al. Size effects on reactivity of Pt nanoparticles in CO monolayer oxidation: The role of surface mobility[J]. Faraday Discussions, 2004, 125: 357-377.

[22] Yano H, Inukai J, Uchida H, et al. Particle-size effect of nanoscale platinum catalysts in oxygen reduction reaction: an electrochemical and ^{195}Pt EC-NMR study[J]. Physical Chemistry Chemical Physics, 2006, 8(42):4932-4939.

[23] Mayrhofer K J J, Blizanac B B, Arenz M, et al.The impact of geometric and surface electronic properties of Pt-catalysts on the particle size effect in electocatalysis [J]. Journal of Physical Chemistry B, 2005, 109 (30): 14433-14440.

[24] Yang H, Tang Y, Zou S. Electrochemical removal of surfactants from Pt nanocubes[J]. Electrochemistry Communications, 2014, 38:134-137.

[25] Aran-Ais R M, Vidal-Iglesias F J, Solla-Gullon J, et al. Electrochemical characterization of clean shape-controlled

Pt nanoparticles prepared in presence of oleylamine/oleic acid[J]. Electroanalysis, 2015, 27(4): 945-956.

[26] Solla-Gullon J, Vidal-Iglesias F J, Lopez-Cudero A, et al. Shape-dependent electrocatalysis: Methanol and formic acid electrooxidation on preferentially oriented Pt nanoparticles[J]. Physical Chemistry Chemical Physics, 2008, 10(25): 3689-3698.

[27] Mayrhofer KJ J, Juhart V, Hartl K, et al. Adsorbate-induced surface segregation for core-shell nanocatalysts[J]. Angewandte Chemie-International Edition, 2009, 48(19): 3529-3531.

[28] Li D, Wang C, Strmcnik D S, et al. Functional links between Pt single crystal morphology and nanoparticles with different size and shape: the oxygen reduction reaction case[J]. Energy & Environmental Science, 2014, 7(12): 4061-4069.

[29] Kitchin J R, Norskov J K, Barteau M A, et al. Modification of the surface electronic and chemical properties of Pt(111) by subsurface 3d transition metals[J]. Journal of Chemical Physics, 2004, 120(21): 10240-10246.

[30] Medford A J, Vojvodic A, Hummelshøj J S, et al. From the Sabatier principle to a predictive theory of transition-metal heterogeneous catalysis[J]. Journal of Catalysis, 2015, 328(S1): 36-42.

[31] Markovic N M, Schmidt T J, Stamenkovic V, et al. Oxygen reduction reaction on Pt and Pt bimetallic surfaces: a selective review[J]. Fuel Cells, 2001, 1(2): 105-116.

[32] Viswanathan V, Hansen H A, Rossmeisl J, et al. Universality in oxygen reduction electrocatalysis on metal surfaces[J]. ACS Catalysis, 2012, 2(8): 1654-1660.

铂合金纳米立方块催化剂的氧还原反应活性比较

汤永安[1,3], 代 琳[1], 邹受忠[1,2*]

(1. 美国迈阿密大学化学与生物化学系,牛津,俄亥俄 45056;2. 美国美利坚大学化学系,
华盛顿特区 20016;3. 美国奥克兰大学化学系,罗切斯特, 密歇根 48039)

摘要: 氧还原反应是质子交换膜燃料电池和金属-空气电池的重要反应. 贵金属铂(Pt)与元素周期表中第一排的非贵过渡金属(M)形成铂合金催化剂(PtM)可以提高氧还原反应活性. 但是,有关活性的提高有多大程度上是来自合金元素的贡献却仍然存在争议. 为研究合金元素对 PtM 催化活性的影响, 本工作合成了颗粒形状与合金元素含量相似的铂锰(PtMn)、铂铁(PtFe)、铂钴(PtCo)和铂镍(PtNi)纳米立方块催化剂,并考察了不同铂合金催化剂在酸性介质中的氧还原反应活性. 选择制备立方块形状纳米颗粒催化剂进行比较,可以将颗粒表面结构对催化活性的影响降到最小. 结果表明,氧还原反应活性与铂 d-能带中心值曲线呈现火山形关系,其中 PtCo 纳米立方块催化剂的活性最高. 本文所得到的实验结果与基于 d-能带理论框架已知表面的密度泛函理论计算结果一致.

关键词: 铂合金纳米立方块; 氧还原反应; 质子交换膜燃料电池; d-能带理论